Journal of Visualization, Vol. 2, Nos. 3/4 (2000) 381-393

Thermographic Investigation of Some Surface Flow Patterns

Carlomagno, G. M.*, Astarita, T.*and Cardone, G.*

* Università degli Studi di Napoli "Federico II," Dipartimento di Energetica, Termofluidodinamica Applicata e Condizionamenti Ambientali (D.E.T.E.C.), P.le Tecchio 80, 80125 Napoli, Italy.
e-mail: carmagno@unina.it

Received 13 September 1999.
Revised 28 September 1999.

***Abstract*:** Infrared (IR) thermography, due to its two-dimensionality and non-contact character, can be usefully employed in a vast variety of heat transfer industrial applications as well as research fields. The present work deals with measurements of temperature and/or convective heat transfer coefficients in several types of fluid flow configurations studied by means of the IR scanning radiometer applied to the heated-thin-foil technique. In more details, it is analysed the capability of the infrared system to study particular phenomena such as: the heat transfer, including the spiral vortical structures developing at transition, over a disk rotating in still air; the thermal exchange enhancement induced by a jet centrally impinging on the rotating disk; the complex heat transfer pattern associated with a jet in cross-flow.

***Keywords*:** flow visualization, infrared thermography, temperature measurements, convective heat transfer.

1. Introduction

The knowledge of convective heat transfer coefficients is of utmost importance for the design of many industrial cooling/heating processes, such as film cooling of turbine blades, anti-icing spray tubes, glass tempering and so forth. Usually, the measure of heat fluxes involves the measure of surface temperatures; in this context, infrared (IR) thermography, which is a measurement technique of thermal maps, can be considered a helpful and innovative technique.

The infrared scanning radiometer (IRSR) consists basically of a camera which detects the electromagnetic energy radiated in the infrared spectral band by an object (whose surface temperature distribution is to be measured and is opaque to the detected band) and converts it into an electronic video signal. This signal is related to the object temperature map.

The IRSR is a true two-dimensional temperature sensor, is non-invasive and so it is advantageous with respect to standard sensors because it does not involve the conduction errors which exist through the wires of thermocouples, or thermistors. The accuracy of the measurement depends mainly on the knowledge of the emissivity coefficient of the surface being viewed by the IR camera; however, an error in the evaluation of the emissivity coefficient generally leads to a smaller error of the measured temperature.

IR thermography can be fruitfully employed to measure convective heat fluxes in both steady and transient techniques; the pertinent heat transfer equation applied to the specific sensor model yields the relationship by which the map of the measured temperatures is correlated to the corresponding distribution of the heat flux rate.

In addition, IRSR allows accurate measurements of surface temperature maps also in presence of high spatial temperature, and/or heat-flux, gradients; its spatial resolution mainly depends on the camera and on the employed optics. Since the IR system measures the object skin temperatures, it can also be regarded as a thin-film sensor or, better, as a two-dimensional array of thin films; however, the response time of IRSR is typically of the

order of $10^{-1} \div 10^{-2}$ s.

As illustrated by Carlomagno (1993-1998a), a fully computerized infrared imaging system, allows for both qualitative and quantitative requirements. In certain applications, as in very fast transients (Simeonides et al., 1989; Henckels et al., 1990), or when dealing with moving objects (Cardone et al., 1994; Astarita et al., 1997), the so-called line-scan option (consisting of locking the vertical scanning mechanism of the radiometer) may be used to decrease the response time, or to reconstruct the thermal image respectively. Of course, in the line-scan mode, unless the object is moving, the measurement is intrinsically one-dimensional.

In the case of an iposonic flow regime ($M<<1$), the aerodynamic heating is not adequate for the IRSR sensitivity, so it is necessary to create a temperature difference between the model surface and the flow, i.e. it is necessary to exchange heat in the so-called active mode. Models of cylindrical geometry (e.g. 2D airfoils, pipes, plates, etc.) can be easily heated by Joule effect by making their surface of a very thin metallic foil, or of a thin printed circuit board. In these cases, the convective heat transfer coefficient from the model surface to the flowing stream is measured by making use of the so-called heated-thin-foil technique. This technique is employed by Carlomagno and co-workers to study several fluid flow configurations which are of industrial and academic interest. In most cases, IR thermography turns out to be an indispensable quick mean to deal with complex fluid-dynamic situations since it allows observation of some particular phenomena; amongst others the laminar-to-turbulent transition, the location and extension of separation bubbles and reattaching regions as well as the formation of azimuthal structures and vortices.

De Luca et al. (1990) characterize the boundary layer development over a wing model to detect transition and separation regions; they relate the measured convective heat transfer data to the wall skin friction by means of the Reynolds analogy. The beginning and the extension of the laminar region, the location of turbulent reattachment points, as well as the regions where the turbulent boundary layer is separated, are quickly identified all over the lee-side surface of the tested wing model even for the case of highly three-dimensional flow.

De Luca et al. (1995) analyse the complex flow pattern, characterized by separation and reattachment lines, over a 65 ° delta wing at different angle of attack from 6 ° up to 30 ° and for the Reynolds number ranging from 1.1×10^6 up to 2.19×10^6. The outward displacement of the secondary separation line, which occurs at the lee-side after transition, as well as shifting of transition with angle of attack and Reynolds number variations are clearly identified.

Carlomagno (1996) performs surface flow visualizations and heat transfer measurements in a backward-facing step flow. In the specific case, the use of the radiometer is found to be particularly advantageous to follow the flow displacement downstream of the step, as the Reynolds number varies from very low values up to 50,000.

Cardone et al. (1997a) analyse the behaviour of a cylinder at angle of attack, having two different blunt fore-bodies (sharp-edged or hemispherical nose), and localise minimum and maximum heat transfer regions associated with separation and reattachment lines.

Astarita et al. succeed in measuring convective heat transfer coefficients in a 180 ° turn static channel (1998a) as well as in a two pass square rotating channel (1998b).

At high Mach numbers, because of the stream high kinetic energy content, the detection of the thermal image may be obtained by the so-called passive mode. Generally, the model initially at uniform ambient temperature, is suddenly exposed to the high total temperature air stream; according to the properly selected thermal model, the thin-skin (e.g. Carlomagno et al., 1991) or the thin-film (e.g. Bynum et al., 1976; de Luca et al., 1992) techniques are used to obtain the convective heat transfer coefficients and/or to investigate the boundary layer behaviour. This method can also be used in the iposonic flow regime by exposing the model to the stream when the former is at an initial temperature which is different from that of the latter one.

However, accuracy of temperature measurements obtained by means of thermography depends on the possibility that all the potential error sources linked to the object, the environment and the acquisition system are reduced. A correct use of infrared thermography involves: characterization of the IR imaging system performance, calibration of the camera, use of additional external optics and/or magnifying mirrors to improve the spatial resolution, determination of the surface emissivity, correct identification of the measured points, design of the optical access window within the choice of the most appropriate IR material. A discussion about these general aspects is reported by Carlomagno and de Luca (1989) and Balageas et al. (1991).

The attention of the present work is focused on the measurement of convective heat transfer coefficients performed by means of infrared thermography applied to the heated-thin-foil technique. The capability of IR thermography to characterize the thermal behaviour of the flow in three different fluid configurations is

highlighted. In particular: the heat transfer, including the spiral vortical structures developing at transition, over a disk rotating in still air; the thermal exchange enhancement induced by a jet centrally impinging on the rotating disk; the complex heat transfer pattern associated with a jet in cross-flow.

2. Steady-state Heated-thin-foil Technique

The heated-thin-foil method consists of uniformly heating a thin metallic foil (or a printed circuit board) by Joule effect and measuring at steady state the convective heat transfer coefficient h from the foil to the stream flowing on it, by means of the relationship:

$$h = \frac{q - q_l}{T_w - T_{aw}} \tag{1}$$

where: q is the known Joule heating flux; q_l represents thermal losses which are mainly due to tangential conduction q_c and radiation q_r ; T_w is the wall temperature which is measured when heating the foil (hot image) and T_{aw} is the adiabatic wall temperature (without heating, cold image).

The foil is generally thermally insulated at its back-face, i.e. the face opposite to that the stream is flowing over. When this insulation cannot be accomplished, e.g. for optical access reasons, additional thermal losses, such as natural convection and radiation on this face, must be taken into account. In this case, the measurement can be generally performed on both sides of the foil; in fact, if the Biot number $Bi=hb/\lambda$ (where λ and b are the foil thermal conductivity and thickness respectively) is relatively small, the foil can be considered isothermal across its thickness.

The tangential conduction q_c, which modulates the thermal signal, may be evaluated by means of the second derivative of the wall temperature T_w. This is relatively easy to perform by taking into account that IRSR yields a very large number of wall temperatures; however, it has to be pointed out that spurious effects linked to the noise have to be avoided by filtering the temperature signal. In the steady state heated-thin-foil technique, the noise can be also strongly reduced by averaging a large number of thermal images acquired in a time sequence.

When the heated-thin-foil is made of a printed circuit board, the bulk tangential thermal behaviour of the foil may be non isotropic. In fact, if the circuit is obtained with several electrical conducting copper tracks arranged in a greek fret mode, the thermal conductance along the copper tracks will be much higher than in the direction perpendicular to them. This may be taken into account, while reducing data, by considering two different equivalent thermal conductivity coefficients λ_p and λ_n, i.e. along the tracks and perpendicularly to them respectively:

$$q_c = b\left(\lambda_p \frac{\partial^2 T_w}{\partial x^2} + \lambda_n \frac{\partial^2 T_w}{\partial y^2}\right) \tag{2}$$

The thermal losses due to radiation q_r may be evaluated according to the Stefan-Boltzman law :

$$q_r = \varepsilon\sigma\left(T_w^4 - T_a^4\right) \tag{3}$$

where ε is the total emissivity coefficient, σ is the Stefan-Boltzman constant and T_a is the equivalent ambient temperature. Under the assumption that the spectral emissivity coefficient ε_λ does not vary much, the total emissivity coefficient ε of the surface under test may be measured by the IR thermography itself by relating the detected radiation from a specimen heated by means of a bath/circulator with its actual temperature monitored by a precise thermometer.

The infrared radiation measured by an IR system can be also affected by atmospheric damping and includes the reflection of energy radiated by the surroundings; these factors may be taken into account by calibration and correction procedures.

Mainly due to the finite dimensions of the IR detector, the modulation, characterized by the Modulation Transfer Function (MTF) of the camera, which produces a signal of decreasing amplitude for increasing the spatial frequency, has also to be taken into account. Moreover, when sampling the analog signal in single detector cameras, a further decrease of the temperature amplitude may be introduced by the analog-to-digital (A/D) converter, which leads to a Sampling Modulation Response.

All the aforementioned effects may reduce, to a greater or a lower extent, the temperature amplitude

according to the experimental conditions, as well as to the measuring sensor, and evidence the need of restoration of the thermal image. This problem is addressed by Carlomagno (1997).

3. Applications

Infrared thermography, applied to the heated-thin-foil technique (Eq.(1)), is employed to study three different fluid flow configurations. Obviously, the measurement of h (i.e. T_w and T_{aw}) involves all the considerations already made in the previous section. In order to enhance the radiated energy, the surface viewed by IR camera is always coated with a thin film of opaque paint whose emissivity factor ε is equal to 0.95 in the bandwidth of interest.

Measurements are performed by means of the AGEMA Thermovision 900LW. The field of view (which depends on the optics focal length and on the viewing distance) is scanned by the Hg-Cd-Te detector in the 8-12 μm infrared window. Nominal sensitivity, expressed in terms of noise equivalent temperature difference, is 0.07 °C when the scanned object is at ambient temperature. The scanner spatial resolution is 235 instantaneous fields of view per line at 50% slit response function. Each image is digitised at 12 bit in a frame of 136 ×272 pixels. For each thermal image, an application software is employed which generally involves: noise reduction by numerical filtering, computation of temperature maps, evaluation of radiation and tangential conduction losses and heat transfer correlation.

3.1 Rotating Disk

The heat exchanged by a disk rotating in still air is of great interest from several practical points of view (Wagner, 1948; Millsaps and Polhausen, 1952; Cobb and Saunders, 1956; Popiel and Boguslawski, 1975; Cardone et al., 1994; Cardone et al., 1997b). The laminar flow due to an infinite flat disk is one of the few exact solutions of the three-dimensional Navier-Stokes equations. Wagner (1948) first evaluates the convective heat transfer coefficient by finding an approximate solution for the laminar regime based on the velocity distribution of von K àrmàn (1921). He finds the following relation between the local Nusselt number Nu_r and Reynolds number Re_r:

$$Nu_r = a\sqrt{Re_r} \tag{4}$$

being the constant a equal to 0.335 for a Prandtl number Pr equal to 0.74 and the local Nusselt and Reynolds numbers defined as:

$$Nu_r = \frac{hr}{k} \tag{5}$$

$$Re_r = \frac{\omega r^2}{v} \tag{6}$$

where r is the local disk radius, ω the rotating speed of the disk and v and k are respectively the kinematic viscosity and the thermal conductivity of air evaluated at film temperature.

Later, Millsaps and Polhausen (1952) solve the exact equation of the thermal field by a similarity solution method and, for the same Pr value, find a value of 0.334 for a. Cobb and Saunders (1956) through an experimental investigation on the mean heat transfer coefficient find that also average Nusselt and Reynolds numbers can be correlated by Eq.(4) with a=0.36, but their Nu_r values at low Re_r are much larger than those predicted by Eq.(4).

Transition to turbulent flow is found to occur at a Reynolds number of about 240,000 (Cobb and Saunders, 1956); the transitional regime is characterized by the presence of spiral counter-rotating vortices (Kobayashi et al., 1980; Kohama, 1984). These vortices are attached to the disk surface and therefore rotate with it.

In the case of turbulent flow and boundary condition of a power law temperature difference ΔT between disk surface and surrounding fluid, Northrop and Owen (1988) obtained the following correlation for the local Nusselt number:

$$Nu_r = 0.0197(n+2.6)^{0.2}\, Pr^{0.6}\, Re^{0.8} \tag{7}$$

where n is the exponent of the power-law temperature difference profile:

$$\Delta T = cr^n \tag{8}$$

c being a constant.

A disk section, which consists of a 450 mm OD steel cup filled with a 20 mm polyurethane foam on which a thin heating printed circuit board is glued, is employed in the present work. Tests are carried out for a Reynolds number Re_r, computed at the disk edge, ranging from 86,000 up to 1,400,000. Details on the experimental apparatus and procedure are reported by Cardone et al. (1997).

A typical two-dimensional thermal image of the disk while is rotating is reported in Fig.1 for Re_r=690,000. As can be seen, nearby the disk centre, the temperature is practically constant since the flow is laminar there; in fact, the constant heat flux boundary condition, due to the unvarying value of h, corresponds to a constant temperature distribution. Moving outward, the temperature decreases sharply in the transitional regime and finally more gradually in the turbulent regime. As the angular speed of the disk increases, the extension of the laminar region reduces and vice versa.

As it will be seen later, the temperature map of Fig.1 is in a sense blurred because of the rotation of the disk; in fact, during the exposure time of the whole image the disk makes more than 2 revolutions and it is not possible to detect the effect of the spiral vortices structures which rotate with the disk.

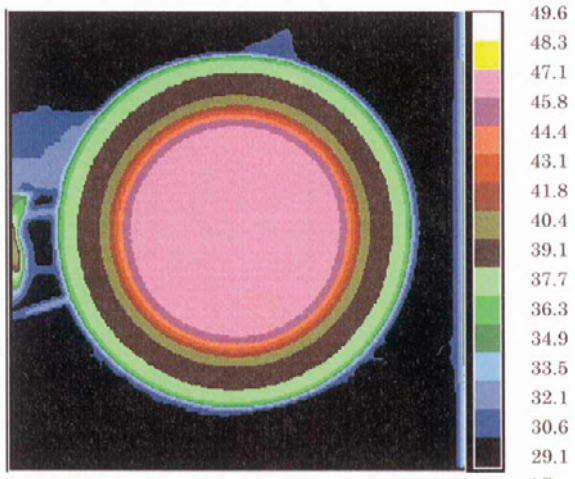

Fig.1. Blurred T_w map for Re_r=690,000.

Data is reduced in non-dimensional form in terms of the local Nusselt number Nu_r where h is calculated from Eq.(1) with q_r evaluated according to the Stefan-Boltzman law Eq.(3) and q_c neglected.

In the laminar regime, the correlation of the present data in terms of Eq.(4) gives a=0.333 which is in very good accordance with literature. Transition seems to occur at Re_r =250,000. A logarithmic regression of data yields in the transitional regime:

$$Nu_r = 8.01 \times 10^{-14} \times Re_r^{2.8} \tag{9}$$

and in the fully turbulent regime:

$$Nu_r = 0.0163 \times Re_r^{0.8} \tag{10}$$

By taking into account that from Eq.(7) the convective heat transfer coefficient h is proportional to $r^{0.6}$ and that, in the case of a constant heat flux boundary condition, ΔT is inversely proportional to h, the coefficient n is equal to −0.6; as a consequence, for Pr=0.71, Equation (7) reduces to:

$$Nu_r = 0.0184 \times Re_r^{0.8} \tag{11}$$

Equation (10) satisfactorily agrees with Eq.(11) and with data of Cobb and Saunders (1956).

Nusselt number values relative to local Reynolds number ranging from 1,000 up to 1,400,000 are shown in Fig.2, together with the solution of Millsaps and Pohlhausen (1952), which is valid for the laminar regime, and the

present regression lines in the transitional and turbulent regimes. The data spread, especially in the laminar regime, appears very contained and much lower than that of previous experiments, which refer to a much smaller Reynolds number range and account for deviation from the theory up to more than 30%.

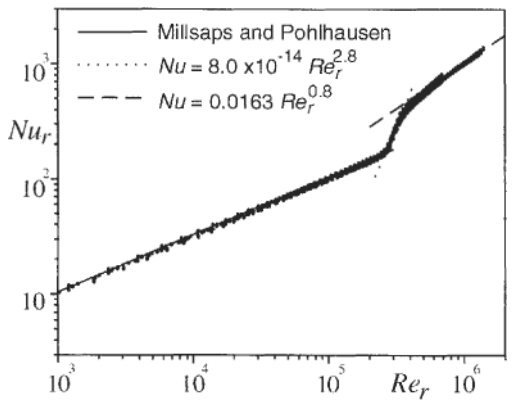

Fig.2. Nusselt number distribution.

The spiral vortices, attached to the disk surface, are detected by means of the line-scan option of AGEMA 900 IR camera; the temperature profile along one radius is obtained as a function of time at thermal steady state. The temperature map on the surface of the rotating disk is reconstructed by taking into account the rotation of the disk, i.e. by azimuthally displacing the different radial profiles so as to generate the steady thermal map connected to the disk surface. The reconstructed map, which is obtained by superimposing about 60,000 radial profiles, is represented in Fig.3.

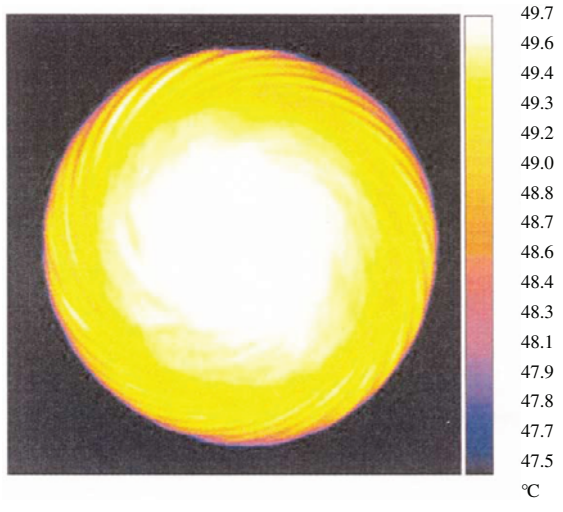

Fig.3. Reconstructed T_w map for Re_r=320,000.

Regions of lower temperature correspond to positions where the velocity vectors of the two adjacent vortices are directed towards the disk and vice versa. The spiral vortices are clearly evident and their number and inclination with respect to the radial direction well agree with previous values reported in the literature.

3.2 Jet Impinging on a Rotating Disk

The same disk described in the previous Section 3.1 is again considered but with a small centred jet impinging on it. The interaction of an air jet with the flow generated by the rotating disk has received little attention (Metzger et al., 1979; Brodersen et al., 1996a,b) and in any case, to the authors' knowledge, the flow configuration of a relatively small centred jet has not been yet considered.

The physical phenomenon is characterized by both the previously defined local Reynolds and Nusselt

numbers based on the disk conditions Nu_r, Eq.(5) and Re_r, Eq.(6), as well those based on the jet conditions Re_j , Nu_j:

$$Re_j = \frac{U_j D}{\nu} \tag{12}$$

$$Nu_j = \frac{hD}{k} \tag{13}$$

where U_j is the jet velocity, D the nozzle exit diameter and h is computed in the same way specified before.

In order to evaluate the relative importance of the jet effect with respect to the disk rotation and on the assumption that the heat transfer coefficient is proportional to the momentum flux, a possible similitude parameter which represents the ratio between the two momentum fluxes, one due to the jet and the other one to the rotation of the disk, may be searched for.

The momentum rate of the jet, is obviously proportional to:

$$\rho U_j D^2 U_j \tag{14}$$

while the rate of momentum induced by the rotating disk is proportional to:

$$\rho \omega r \quad r\delta \quad \omega r \tag{15}$$

where δ is the local boundary layer thickness. Of course, an appropriate local radius r has to be chosen.

The present testing conditions involve relatively high values of impingement distance z, as compared to nozzle diameter D, and as it is well known, under these circumstances, the width of the jet is proportional to the distance from the nozzle.

By taking into account that, for laminar flow on a rotating disk, the boundary layer thickness is constant and proportional to the square root of the ratio between the kinematic viscosity coefficient and the angular speed of the disk and by substituting in Eq.(15) the local radius with the semi-width of the jet (which in turn is proportional to z) the searched similitude parameter, proportional to the momentum rates ratio, becomes equal to:

$$\xi^2 = Re_j^2 \left(\frac{\nu}{\omega z^2} \right)^{\frac{3}{2}} = \frac{Re_j^2}{Re_r^{3/2} \left(\frac{z}{r} \right)^3} \tag{16}$$

The experimental apparatus which is used in the present tests is the same exploited for those of the previous section. Three nozzles of exit diameter 4, 6 and 8 mm are employed, the air flow rate issuing from them is varied in the range 0.91-4 m^3/h and their distance from the disk is varied between 15 and 75 nozzle diameters. The bulk temperature of the low initial Mach number jet is practically kept equal to the temperature of the ambient air it mixes with. In the present experiment, the adiabatic wall temperature is therefore considered to coincide with the ambient temperature and consequently with the jet bulk one.

The temperature map relative to the disk rotating at 865 rpm, heated with a heat flux q=1,080 W/m^2, with a centred impinging jet of Re_j=3,500, is shown in Fig.4 for a Reynolds number at the disk edge Re_r =292,000, ξ= 0.062 and of dimensionless nozzle to plate distance z/D=75. As can be seen, the temperature distribution is practically constant; because of the relatively large impingement distance and the small jet Reynolds number, the jet influence is restricted only to a very small zone nearby the disk centre and the rotation effects dominate the flow. The change of colour nearby the disk contour is mainly due to an edge effect.

If heat flux losses q_l are neglected in Eq.(1), each temperature level in the map is practically inversely proportional to the convective heat transfer coefficient; therefore higher temperatures correspond to lower heat transfer coefficients and vice versa.

If the disk angular speed is slightly decreased (to be sure that the maximum Re_r is below 250,000) from 865 rpm to 720 rpm while the heat flux is increased to q=1,547 W/m^2 and if the jet impinges at a shorter distance z/D = 18.4 and with a higher Reynolds number Re_j = 10,100, the temperature distribution appears completely modified as Figure 5 shows.

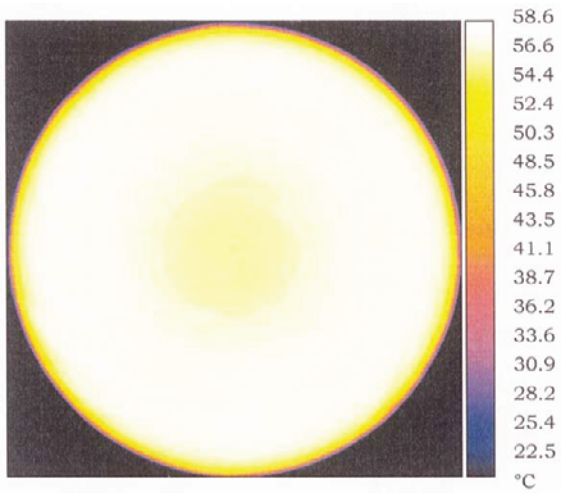

Fig.4. T_w map; Re_r=292,000, Re_j=3,500, z/D=75.

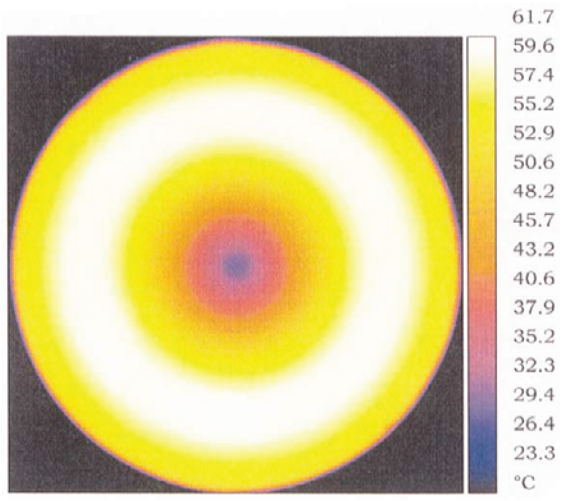

Fig.5. T_w map; Re_r=248,000, Re_j=10,100, z/D=18.4.

Moving from the disk centre outwards, the temperature initially rapidly increases, reaches a local maximum and then slowly decreases towards the disk edge. Consequently, the local convective heat transfer coefficient undergoes an absolute minimum at about 70% of the disk radius. The increase of the heat transfer coefficient towards the disk edge may be only attributed to the interaction of the turbulent jet with the laminar disk boundary layer. In fact, the turbulence of the jet, together with the increase of the radial velocity component due to the jet presence, tends to shift the transitional instability on the disk towards lower values of the local Reynolds number Re_r, i.e. towards lower local radii. Since the temperature map of Fig.5 is again obtained by means of the line-scan option, one may also conclude that the jet presence makes the spiral vortices (already found for the rotating disk without the jet) disappear.

By comparing Fig.5 to Fig.4, it can be observed that the heat transfer coefficient, at the disk centre, is significantly increased. This can be easily verified from Eq.(1) by taking into account both the lower wall temperature and the higher Joule heat flux.

As far as the heat transfer coefficient is concerned, for $0.1 \leq \xi \leq 1$, present data leads to a correlation between the Nusselt number and the Reynolds number at the disk centre (stagnation point) that can be written as:

$$\left(\frac{Nu_r}{\sqrt{Re_r}}\right)_{r=0} - 0.33 = 1.58\xi \tag{17}$$

which has a good correlation coefficient (R^2=0.988) and, for $\xi \to 0$, reduces to the classical relationship between the local Nusselt and Reynolds numbers for a laminar boundary layer over a rotating disk (see Sec. 3.1). Instead for $1 \leq \xi \leq 100$ data is well correlated by equation:

$$\left(\frac{Nu_r}{\sqrt{Re_r}} \right)_{R=0} - 0.33 = 1.55 \xi^{0.64} \tag{18}$$

The two above correlations, which practically coincide for ξ=1, are shown in Fig.6 together with the experimental measurements.

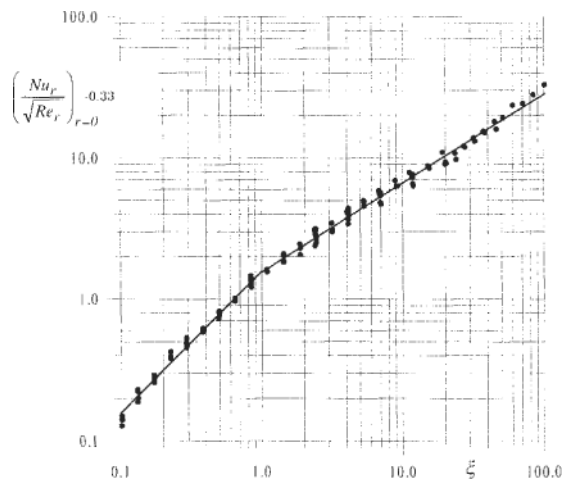

Fig.6. Experimental data correlation for the impinging jet.

For $\xi > 2$, all the experimental profiles of the heat transfer coefficient along the disk radius, reported in terms of the dimensionless parameter $Nu_r / \sqrt{Re_r}$ normalised with respect to $(Nu_r / \sqrt{Re_r})_{r=0}$ against r/z, tend to overlap for r/z<0.8. However, for increasing r/z and according to the tested conditions, many of the curves show an increasing convective heat transfer coefficient. This effect may again be ascribed to the interaction of the turbulent jet with the laminar boundary layer generated by the rotating disk that, inducing an earlier transition, enhances the heat exchange at high r/z.

3.3 Jet in Cross-flow

A jet discharging normal to a cross-flow gives rise to a complex interaction between the two flows resulting in the deflection of the jet in the direction of the cross-flow; the cross-sectional area increases as the jet entrains fluid from the external stream and assumes a horseshoe shape with a pair of counter-rotating trailing vortices (Andreopoulus and Rodi, 1984; Coelho and Hunt, 1989; Kelso et al., 1996; Carlomagno et al., 1998b). In addition, ring-like vortices are present in the shear layer wall which become distorted with streamwise distance; the wake region beneath the downstream side of the jet contains streamwise wall vortices that lie above the flat wall and vertically oriented shedding vortices.

In the present work, attention is focused on the measurement of the convective heat transfer coefficients over the flat wall the jet is issuing from. In particular, the combined effects of the free stream and the jet perpendicularly injected into it for a given stream velocity, U_∞, and by varying the injection ratio, $R=U_j/U_\infty$ (where U_j is the jet mean velocity at nozzle exit) is analysed.

Tests are carried out in an open circuit wind tunnel having a 300 $\times$400 mm^2 test section which is 1,100 mm long and characterized by a very low turbulence level ($\cong$0.1%); one side wall of the tunnel is made of a thin printed circuit board insulated at the back and with a centred hole, drilled at 200 mm from the plate edge (i.e. the tunnel throat), for the jet injection; the electrical continuity for the Joule heating is assured by welding points over the copper tracks (4.5 mm wide) near the hole edge. The access window to the test section for the infrared camera is simply made of bioriented polyethylene; calibration of the radiometer takes into account its presence. The air jet issues from a circular nozzle of exit diameter D=13.7 mm; air, supplied by a compressor, goes through a pressure-regulating valve, a heat exchanger, a flow-meter, then to a plenum chamber where the temperature is metered and

so through the nozzle into the wind tunnel section.

Tests are carried out for U_∞=5 m/s and R values ranging from 1 to 5. Particular care is taken to maintain, during tests, the plenum jet temperature equal to the ambient one, which coincides with the stream temperature. Maps of T_w, for R=1 and 5, are shown in Fig.7. As can be seen, outside of the wake induced by the jet, the development of the boundary layer over the plate, with increasing wall temperature in the downstream direction, is clearly observable; furthermore, as R increases the isotherms tend to wrap around the nozzle exit and to diverge downstream.

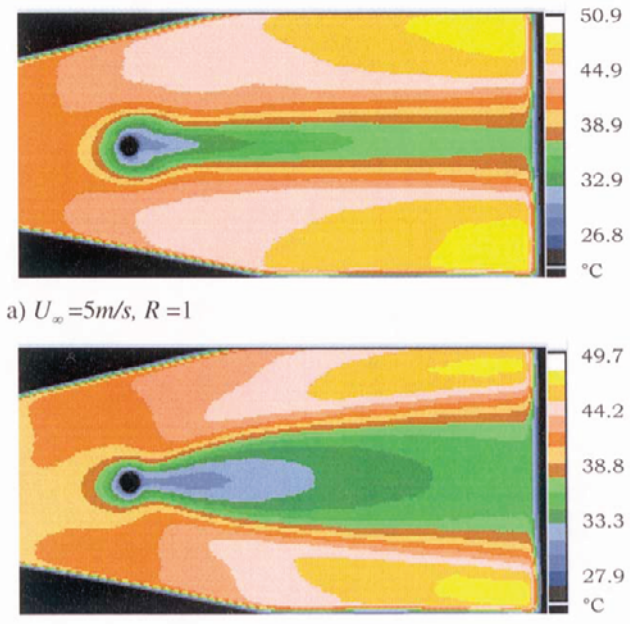

Fig.7. T_w maps.

It has also to be pointed out that, due to the averaging process and to the relatively high thermal inertia of the foil, the temperature maps of Fig.7 depict only an average situation, i.e. cannot represent the fluctuating behaviour of the flow. This is one of the major limitation of the thermographic measurements when studying turbulent flows.

Data is reduced in non-dimensional form in terms of the Nusselt number Nu based on the nozzle exit diameter D:

$$Nu = \frac{hD}{k} \tag{19}$$

where h is computed from Eq.(1) with losses, due to conduction and radiation, evaluated according to Eq.(2) and Eq.(3) respectively. In particular, Nu is normalised with respect to the measured Nu_o, i.e. the Nusselt number relative to the undisturbed plate without jet injection and with the hole closed to simulate the case of a flat plate. The maps of the Nusselt ratio Nu/Nu_o for U_∞=5 m/s and R=1, 3 and 5 are shown in Fig.8; a circle denotes the position of the jet exit.

In general, Nu/Nu_o takes values equal to unity outside the jet wake where heat transfer is influenced only by the stream; immediately downstream of the injection hole a low heat transfer zone is present, further downstream the Nusselt number increases and attains its maximum value at about X/D=1.75 starting from the nozzle centre. A secondary peak, less pronounced than the first one is located at about 3.25 diameters downstream regardless of the injection ratio R.

Goldstein and Taylor (1996), by employing an array of jets inclined at 35° with respect to the direction of the main flow, found a maximum heat transfer value at about 0.75 D starting from the nozzle edge; furthermore, their maximum Nusselt ratio is rather lower (about 3.5) with respect that (about 6) of present tests. Differences are to be principally ascribed to the different nozzle geometry.

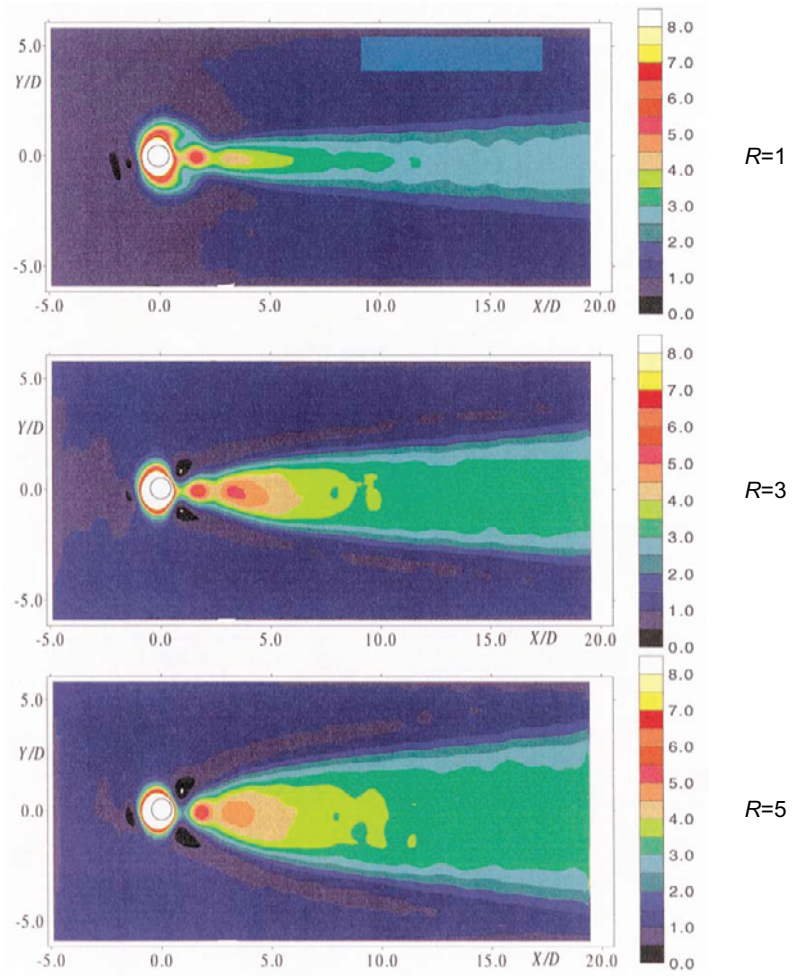

Fig.8. Maps of Nu/Nu_o.

According to literature, the minimum heat transfer value at about 1 D may be ascribed to the stagnation region created by the injection. The maximum instead may be associated with the formation of eddies in the wake region; in fact, as the jet separates from the wall, for increasing R, the mainstream flow penetrates beneath the jet giving rise to the formation of the wake vortices which entail high local heat transfer. The two lateral Nu/Nu_o minima at about 1 D should correspond to the position of the two trailing vortices which accompany the jet issuing from the nozzle.

It has to be pointed out that the presence of the welding points over the copper tracks disturbs the T_w distribution nearby the hole contour and does not allow for a correct interpretation of results in that region. To study the zone close to the nozzle edge and eventually visualize the horseshoe vortices, a new appropriate circuit without welding points was constructed and tests are still under way.

4. Conclusions

Infrared thermography applied to the heated-thin-foil technique is employed to perform convective heat transfer measurements in some fluid flow configurations.

Particular phenomena associated with the flow dynamics are detected such as: the presence of spiral vortices in the transitional regime of the flow of a disk rotating in still air; the interaction between the jet and the boundary layer which is developed by the disk rotation; heat transfer developing in the wake region of a jet in cross-flow.

Data for the rotating disk shows a very low scattering over a very wide range of Reynolds number, confirms with a great accuracy the theoretical result for the laminar regime and gives new correlations for the transitional and turbulent one.

The line-scan option of IRSR allows for visualizations of the spiral vortices in the transitional regime of the

rotating disk; the temperature distribution over the whole disk surface is reconstructed by azimuthally displacing the radial profiles so as to generate the steady thermal map rotating with the disk surface. The number and inclination of the spiral vortices well agree with previous values reported in the literature.

The influence of the impinging air jet on the flow generated by the rotating disk is evaluated through a similitude parameter as ratio between the momentum flux due to the jet and the momentum flux due to the rotation of the disk. The introduction of this parameter allows for a correlation between the Nusselt number and the Reynolds number at the stagnation point. It is also found that the presence of the jet induces an earlier transition of the boundary layer and that this spiral vortices disappear in this circumstance.

Data relative to a jet normally discharging into a cross-flow shows that immediately downstream of the injection hole a low heat transfer zone is present, further downstream the Nusselt number increases and attains its maximum value at about X/D=1.75 starting from the nozzle centre; a secondary peak, less pronounced than the first one is located at about 3.25 diameters downstream regardless of the injection ratio R. According to literature, the minimum heat transfer value at about 1 D may be ascribed to the stagnation region created by the injection, the maximum instead may be associated with the formation of eddies in the wake region; in fact, as the jet separates from the wall, for increasing R, the mainstream flow penetrates beneath the jet giving rise to the formation of the wake vortices which entail high local heat transfer.

Results prove that the infrared radiometer is a powerful tool; however, precise quantitative measurements require that all the potential error sources and modulations should be reduced and the most appropriate testing procedure to the specific flow configuration adopted.

References

Andreopoulos, J. and Rodi, W., "Experimental investigation of jets in a cross-flow," J. Fluid Mech. 138 (1984).

Astarita, T., Cardone, G. and Carlomagno, G. M., "IR heat transfer measurements in a rotating channel," on Proceedings of the S eminar on Quantitative Infrared Thermography (QIRT 96), Balageas, D., Busse, G. and Carlomagno, G.M. eds, (1997).

Astarita, T., Cardone, G. and Carlomagno, G. M., "Average heat transfer measurements near a sharp 180° turn channel for differe nt aspect ratios," Optical Methods and Data Processing in Heat and Fluid Flow, ImechE Conf. Trans., London (1998a).

Astarita, T., Cardone, G. and Carlomagno, G. M., "Heat transfer measurements in a rotating two pass square channel," The 7th In t. Symposium on Transport Phenomena and Dynamics of Rotating Machinery, Hawaii (1998b).

Balageas, D. L., Boscher, D. M., Deom, A. A., Fournier, J. and Gardette, G., "Measurement of convective heat transfer coefficie nts in wind tunnels using passive and stimulated infrared thermography," Rech. Aerosp., 1991-4 (1991).

Brodersen, S., Metzger, D. E. and Fernando, H. J. S., "Flows generated by the impingement of a jet on a rotating surface: Part I-Basic flow patterns," J. of Fluid Engineering, 118 (1996).

Brodersen, S., Metzger, D. E. and Fernando, H. J. S., "Flows generated by the impingement of a jet on a rotating surface: Part II-Detailed flow structure and analysis," J. of Fluid Engineering, Vol.118.

Bynum, D. S., Hube, F. K., Key, C. M. and Diek, P. M., "Measurement and mapping of aerodynamic heating with an infrared camera, " AEDC Rept. TR-76-54 (1976).

Cardone, G., Astarita, T. and Carlomagno, G. M., "Infrared thermography to measure local heat transfer coefficients on a disk r otating in still air," Proceedings of the Workshop Advanced Infrared Technology and Applications, Baccini & Baldi, Firenze (1994).

Cardone, G., Buresti, G. and Carlomagno, G. M., "Heat transfer to air from a yawed circular cylinder," in Atlas of Visualization, Y. Nakayama and Y.Tanida eds., (1997a), Vol. III, Chap.10, CRC Press.

Cardone, G., Astarita, T. and Carlomagno, G. M., "Heat transfer measurements on a rotating disk", Int. J. Rotating Machinery, 3 (1997b).

Carlomagno, G. M. and de Luca L., "Infrared thermography in heat transfer," in Handbook of Flow Visualization, (ed. W.J. Yang), (1989) ,Chap. 32, Hemisphere.

Carlomagno, G. M., de Luca, L. and Alziary de Roquefort, T., 1991, "Mapping and measurement of aerodynamic heating and surface flow visualization by means of IR thermography," in Multiphase Flow and Heat Transfer, (Eds. Chen et al.), Vol. 2, Hemisphere.

Carlomagno, G. M., "Heat transfer measurements by means of infrared thermography," in Measurement Techniques, von Karman Instit ute for Fluid Mechanics Lect. Series 1993-05 (1993), Rhode-Saint-Genese.

Carlomagno, G. M., "Surface flow visualization of a backward-facing step flow," in Atlas of Visualization II, Y. Nakayama and Y. Tanida eds., (1996), Chap.7, CRC press, New York.

Carlomagno, G. M., "Thermo-fluid-dynamic applications of quantitative infrared thermography," Proceedings of the 1st Pacific Sy mposium on Flow Visualization and Image Processing Vol. 1, Honolulu (1997).

Carlomagno, G. M., Cardone, G., Meola, C. and Astarita, T., "Infrared Thermography as Tool for Thermal Flow Visualization", J. of Visualization, 1 (1998a).

Carlomagno, G. M., Cenedese, A. and De Angelis, G., "PTV analysis of jets in cross-flow," Proc. 9th Int. Symp. on Applications of Laser Techniques to Fluid Mechanics, Vol. 2, 38.3 1-38.3 7, Lisbon (1998b).

Cobb, E. C. and Saunders, O. A., "Heat transfer from a rotating disk," Proc. Royal Society, Vol. 236 (1956).

Coelho, S. L. V. and Hunt, J. C. R., "The dynamics of the near field of strong jets in cross flows," J. Fluid Mech. 200 (1989).

De Luca, L., Carlomagno, G. M. and Buresti, G., "Boundary layer diagnostics by means of an infrared scanning radiometer," Exper iments in Fluids, 9 (1990).

De Luca, L., Cardone, G., Carlomagno, G. M., Aymer de la Chevalerie, D. and Alziary de Roquefort, T., "Flow visualization and h eat transfer measurement in a hypersonic wind tunnel," Experimental Heat Transfer, 5 (1992).

De Luca, L., Guglieri, G., Cardone, G., Carlomagno, G. M., "Experimental analysis of surface flow on a delta wing by infrared t hermography," AIAA Journal 33, 8 (1995).

Goldstein, R. J. and Taylor, J. R., "Mass transfer in the neighbourhood of jets entering a cross flow," J. Heat Transfer, 104 (1982).
Henckels, A., Maurer, F., Olivier, H. and Gronig, H., "Fast temperature measurement by infrared line scanning in a hypersonic s hock tunnel," Experiments in Fluids, 9 (1990).
Kelso, R. M., Lim, T. T. and Perry, A. E., "An experimental study of round jets in cross-flow," J. Fluid Mech., 306 (1996).
Kobayashi, R., Kohama, Y. and Takamadate, C., "Spiral vortices in boundary layer transition regime on a rotating disk," Acta Mech., 35 (1980).
Kohama, Y., "Study on Boundary Layer Transition of a Rotating Disk," Acta Mech., 50 (1984).
Metzger, D. E., Mathis, W. J. and Grochowsky, L. D., 1979, "Jet cooling at the rim of a rotating disk," J. of Engineering for Power, 101 (1979).
Millsaps, K. and Pohlhausen, K., "Heat transfer by laminar flow from a rotating plate," J. Aeronautical Science, 19 (1952).
Nelson, R. C., Unsteady aerodynamics of slender wings," AGARD Rept 776, (1991).
Northrop, A. and Owen, J. M., "Heat transfer measurements in rotating-disk systems. Part.1: The free disk," Int. J. Heat and fl uid Flow, 9, 1 (1988).
Popiel, Cz. O. and Boguslawski L., "Local heat transfer coefficients on the rotating disk in still air," Int. J. Heat and Mass Transfer, 18 (1975).
Simeonides, G., Van Lierde, D. P., Van der Stichele, S., Capriotti and Wendt, J.F., "Infrared thermography in blowdown and inte rmittent hypersonic facilities," AIAA Paper 89-0042 (1989).
Von Kàrmàn, T., "Laminare und Turbulente Reibung," ZAMM, Vol.1 (1921).
Wagner, C., "Heat transfer from a rotating disk to ambient air," J. Applied Physics, 19 (1948).

Author Profile

Giovanni Maria Carlomagno: He became Doctor in Mechanical Engineering (summa cum laude) in 1965, Research assistant at University of Princeton (1967-68), Associate professor of Physics (1969), Associate Professor of Gasdynamics (1975), Professor of Aerospace and Mechanical Enginnering (1986). He has chaired 14 International Meetings, is editor of 14 books and author of some 200 scientific papers on Aerodynamics, Gasdynamics, Heat transfer, Fluidics, Non-newtonian fluid dynamics, Measurement techniques in thermo-fluid-dynamics, Tethered satellites, Infrared thermography, Image Processing. He is Member of the Advisory Board of the Pacific Center of Thermal-Fluids Engineering, the Scientific Council of the International Centre for Heat and Mass Transfer and of the Executive Committee of the International Council for Aeronautical Sciences, Member of the Editorial Board of more than 10 International Scientific Journals, Chairman of the Technical Advisory Committee of the von Karman Institute and Dean of the school of Aerospace Engineering of the University of Naples.

Tommaso Astarita: He received his master degree in Aeronautical Engineering (summa cum laude) in 1993 and PhD in Aerospace Engineering in 1997 at University of Naples. He is an expert in Infrared Thermography applied to convective heat transfer problems and is an author of some 20 scientific papers in this field. His more recent research interest includes the application of PIV techniques to fluid dynamics.

Gennaro Cardone: He graduated with summa cum laude in Mechanical Engineering (1988), and received PhD in Aerospace Engineering at University of Naples (1991). He was an Assistant Professor at the University of Naples from 1992 to 1998, and has been an Associate Professor of Fluid Mechanics at the University of Naples since 1998. His major research fields are: Two-beam and reference beam interferometry; Application of the Infrared Thermography to quantitative measurements of heat transfer coefficients and flow fields visualization; Aerodynamic heating and visualization of flow fields in hypersonic flow; Viscous interaction and Goertler vortices in hypersonic flow; Boundary layer diagnostic and visualization of subsonic flow fields; Internal flow in the laminar, transitional and turbulent regimes. He is an author of more than 50 scientific publications.